scientific reports

Check for updates

OPEN

Smart extrusion via data-driven prediction of grain size and peripheral coarse grain defect formation

Marco Negozio[1✉], Lorenzo Donati[2] & Adrian H. A. Lutey[1]

Optimization of the mechanical and crash properties of extruded AA6XXX automotive profiles requires detailed understanding of grain size evolution and formation of the peripheral coarse grain (PCG) defect. Conventional approaches demand extensive experimental campaigns which, further to being lengthy and resource-intensive, often lead to the adoption of conservative process parameters that limit production efficiency. The present work proposes a data-driven method for predicting grain size and PCG formation, combining finite element method (FEM) simulation data with experimental microstructural observations to train machine learning (ML) algorithms for classification and regression. Over 22,000 data points were collected from two distinct AA6082 aluminum alloy profiles with different geometries, extruded over a range of different process conditions. Hyperparameter optimization of artificial neural networks (ANNs) for regression and prediction was performed, with ANN outcomes benchmarked against existing analytical models. PCG formation was predicted with 5.8% false negatives and 3.9% false positives compared to 10.1% and 18.1%, respectively, with existing analytical models, while grain size was predicted with a mean squared error (MSE) of 9.77 μm^2 compared to 48.3 μm^2. PCG and grain size maps were then produced to demonstrate how prediction of grain size and PCG formation can be employed in a smart manufacturing environment.

The extrusion of AA6XXX aluminum alloy profiles for the automotive industry is crucial due to requirements for excellent strength, formability and corrosion resistance. As automakers focus on producing lighter, more fuel-efficient vehicles, the demand for advanced materials that meet stringent performance standards is increasing. Ensuring the properties of extruded materials by controlling their chemical composition and microstructure is essential for achieving consistent, reliable and optimal mechanical properties and crash performance. Such control is challenging, however, due to interplay between the temperature and pressure during extrusion, as well as complex material flow at high strain, differential cooling rates, alloy composition effects and equipment variability[1]. Each of these factors must be managed to achieve the desired material properties, making production inherently complex and often inefficient.

A peripheral coarse grain (PCG) structure is a recurring microstructural defect that occurs during the extrusion of Al-Mg-Si automotive alloys such as AA6005A and AA6082, which is particularly problematic for guaranteeing the crash properties of the resulting profiles. The defect appears as a surface layer of large, recrystallized grains that undermine the crash properties of the extruded profile by facilitating crack formation during profile compression, reducing the mean crash force (MCF) and corrosion resistance[2], thereby severely limiting component suitability for automotive applications. Eliminating the occurrence of a PCG layer is one of the most significant challenges in the aluminum extrusion industry; however, addressing this issue is challenging because the formation of coarse grains in extruded aluminum alloys arises from complex interplay between alloy composition, homogenization, extrusion and quenching parameters[3].

To minimize PCG defects in AA6XXX alloys, one effective strategy is to control both the chemical composition and alloy homogenization process. The addition of elements like Mn, Cr, or Sc promotes the formation of dispersoids, which inhibit recrystallization and reduce PCG risk but can decrease formability, as highlighted by Rakhmonov et al.[4]. Goik et al.[5] demonstrated that in AA6082, high dispersoid concentration limits grain boundary migration, producing a fine-grained microstructure and reducing the PCG layer. Similarly, Fangzhen et al.[6] found that an optimal Mn ratio (3.5:1) enhances dispersoid formation and improves both

[1]Department of Engineering for Industrial Systems and Technologies (DISTI), University of Parma, Parco Area delle Scienze, 181/A, 43124 Parma, Italy. [2]Department of Industrial Engineering (DIN), University of Bologna, Viale Risorgimento 2, 40136 Bologna, Italy. ✉email: marco.negozio@unipr.it

mechanical properties and thermal stability, while excessive Cr diminishes this effect. Research by Sandi et al.[7] on Sc additions in AA6086 further emphasized the role of microalloying elements in refining microstructure. In relation to homogenization, Österreicher et al.[8] and Qian et al.[9] found that lower homogenization temperatures and shorter soak times lead to finer dispersoid distribution, improving PCG resistance. Zhen et al.[10] showed that a two-step homogenization process enhances dispersoid uniformity and reduces coarse dispersoid zones, further improving PCG resistance.

Another approach to controlling PCG formation focuses on optimizing extrusion and quenching parameters. Eivani et al.[11] highlighted that local high temperatures, more than strain rates, drive PCG formation during extrusion, showing that controlling ram speed and billet temperature can significantly impact the PCG layer. Zhao et al.[12] instead proposed that higher billet temperatures and faster ram speeds increase PCG layer thickness, with the profile surface experiencing higher strain and strain rates compared to the core. Mahmoodkhani et al.[13] demonstrated that using choke angles in die bearings can reduce PCG formation by lowering the maximum strain rate, suggesting that strain rate is more critical than exit temperature. De Peri and Misiolek[14] and Misiolek and Van Geertruyden[15] supported this by linking PCG behavior to very fine grains within the outer layers of extruded profiles, attributed to geometric or continuous dynamic recrystallization (gDRX/cDRX). Eivani et al.[16] expanded on this by proposing that large second-phase particles, coupled with high surface strains and strain rates, promote static recrystallization (SRX), which forms larger grains on the surface compared to the inner PCG layer.

Few authors have proposed predictive models for PCG formation, which is a major limiting factor for optimizing production efficiency. Mahmoodkhani et al.[13] proposed a model based on stored energy, built into a finite element method (FEM) simulation of Al-Mg-Si-Mn alloy extrusion. Eivani et al.[17] simulated microstructural evolution during hot extrusion of AA7020 aluminum alloy using multiscale physical models, combining FEM and Monte Carlo simulations. Despite significant advancements in knowledge relating to the mechanisms of PCG formation and prevention strategies, experimental and numerical studies to date have been limited to round bar extrusion in laboratory conditions, largely restricting the range of process conditions considered and hindering broader validation of the proposed theories. The only predictive model for PCG to be tested on experimental cases other than round bars and for various combinations of process parameters was that developed by Negozio et al.[18], in which the formation of PCG was correlated with high values of strain rate, temperature and percentage dynamic recrystallization. This model was tested on two AA6082 alloy profiles, providing good qualitative prediction of outcomes; however, no quantitative assessment was performed to determine the exact accuracy of the model.

These conditions suggest exploration of data-driven modeling to account for the complex interplay between extrusion conditions, grain size distribution and PCG formation. Machine learning (ML) algorithms are known to be well suited to multidimensional problems with low transparency[19], implying that their implementation alongside analytical and numerical models for prediction of grain size and PCG formation during hot extrusion could potentially improve accuracy and help reduce time and cost requirements during the development of new profiles and materials, further to facilitating optimization of production efficiency. ML has found a wide range of applications in manufacturing and metal forming. Cui et al.[20] applied a backpropagation neural network (BPNN) and genetic algorithm (GA) to predict softening kinetics and rolling forces during hot rolling of steels, demonstrating that ML algorithms could achieve higher accuracy than traditional models. Ding et al.[21] applied explainable artificial intelligence (XAI) to cold rolling, employing physics-based and controller parameters to achieve improvements in flatness prediction compared to previous ML methods while assessing the average impact of input parameters on model accuracy via Shapley additive explanations (SHAP). In the field of extrusion, an early work by Hsiang et al.[22] saw the application of artificial neural networks (ANNs) to the prediction of the tensile strength of hot extruded magnesium alloy. Zhou et al.[23] then developed an ANN model for the prediction of extrusion load and exit temperature of magnesium alloy. Bingöl et al.[24] developed an ANN model for predicting extrusion load, while Abdul Jawwad and Barghash[25] developed an ANN-based model for the prediction of maximum extrusion pressure, achieving higher accuracy than previous models. Almutahhar et al.[26] instead developed an ANN model for the prediction of extrusion die failure modes. ML algorithms have also seen application to extrusion of polymers and adhesives for angle estimation during the manufacturing of microcatheter tubes via convolution neural networks (CNNs)[27] and prediction of tensile properties during additive manufacturing via active learning based on the Gaussian process regression algorithm[28].

Within this context, the present work combines FEM simulations and ANN models to predict grain size and PCG formation within extruded aluminum alloy profiles destined for the automative industry, providing a pathway for increasing production efficiency by improving prediction accuracy, reducing the required number of experiments and allowing a more complete assessment of parameters affecting mechanical and crash properties. The microstructures of various extruded profiles characterized by PCG formation have been analyzed in detail to provide a dataset of more than 20,000 entries, with FEM simulations performed in Qform Extrusion UK with customized subroutines to determine potentially relevant parameters influencing recrystallization of aluminum alloy. To minimize the risk of inherent errors introduced by FEM simulations negatively affecting ANN model performance, each simulation has been validated against experimentally acquired data such as the profile exit temperature and extrusion load to ensure that numerical predictions represent the physical process as closely as possible. Extensive ANN hyperparameter optimization has been performed to provide reliable predictions of grain size and PCG formation with the lowest possible loss, or error. The outcomes of this study imply that data driven models have the potential to predict grain size and PCG formation with greater accuracy than existing analytical models, with little additional complexity in their implementation and greater versatility in applying standardized procedures for training new models based on limited experimental data. Unlike previous models, typically limited to simple geometries or a narrow range of process parameters, the developed methodology captures the complex, high-strain behavior inherent to industrial extrusion, thereby enabling precise prediction

Alloying element [Wt%]	Si	Fe	Cu	Mn	Mg	Cr	Ni	Zn
	1.00	0.20	0.03	0.49	0.62	<0.01	<0.01	0.01

Table 1. Chemical composition of AA6082 aluminum alloy employed for experiments.
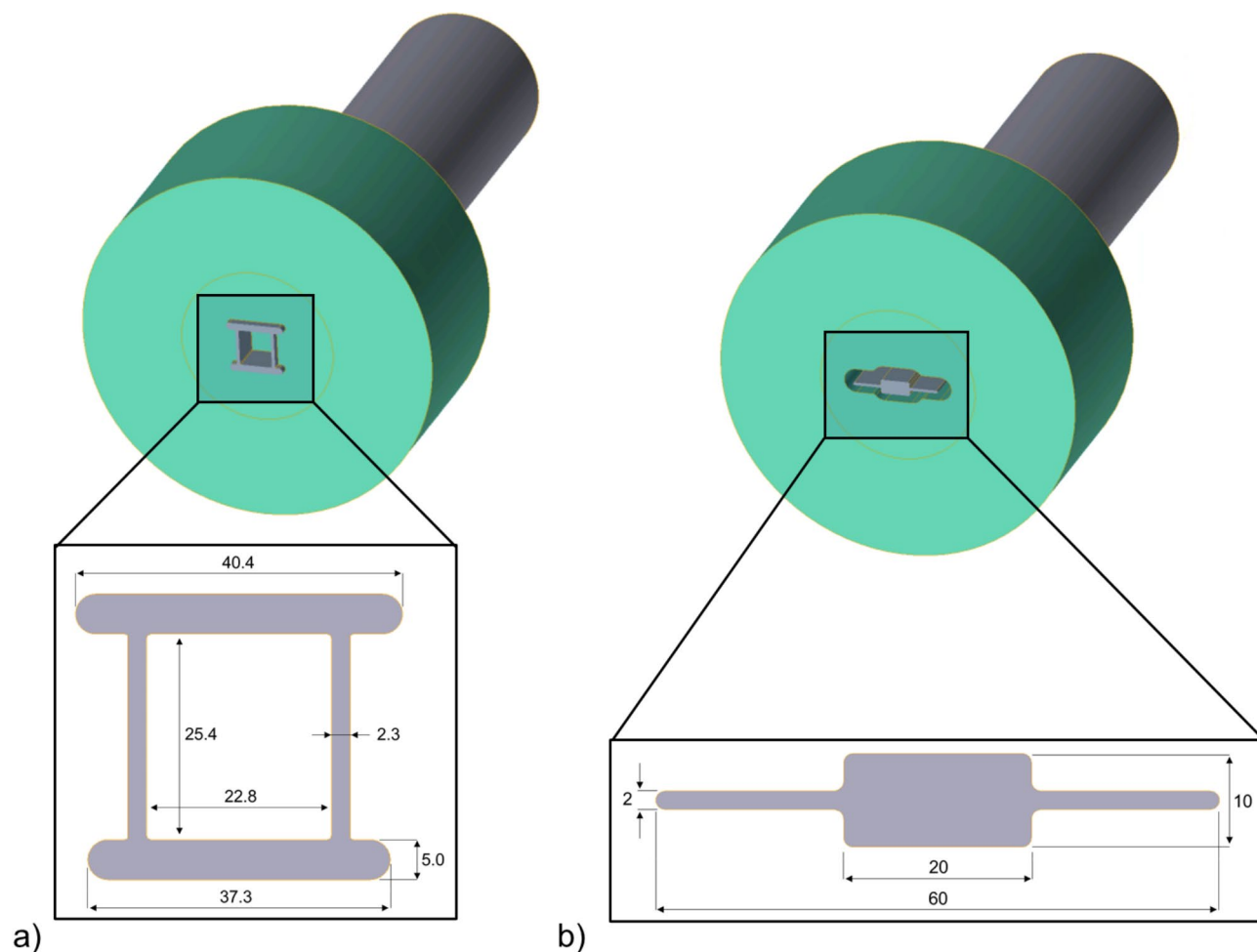
**Fig. 1**. Geometry of extruded profiles used for experiments: (**a**) Profile A, (**b**) Profile B.

of microstructural evolution in AA6XXX alloys. This study is the first to apply an integrated FEM-ANN framework to extruded automotive profiles, simultaneously predicting both grain size and peripheral coarse grain formation.

Materials and methods
Extrusion and micrograph analysis
PCG formation is a phenomenon that generally occurs in AA6XXX alloys with higher alloy content and superior mechanical properties than other aluminum alloys. Specifically chosen for this investigation, AA6082 alloy exemplifies these characteristics with the chemical composition detailed in Table 1. Two AA6082 profiles with geometry as shown in Fig. 1 were extruded at Hydro in Finspång, Sweden, using a 10 MN extrusion press. Profile A was a hollow profile with two thicker horizontal and two thinner vertical walls. Profile B was a solid section with a central area of greater thickness and two thinner lateral fins.

Both investigated profiles were extruded using a wide variety of process parameters to generate a comprehensive dataset for calibration and validation of the developed prediction models. Profile A, with an extrusion ratio of 18.2, was extruded with two billet preheating temperatures, 450 °C and 500 °C, and three ram speeds, 2 mm/s, 5 mm/s, and 10 mm/s. Profile B, with an extrusion ratio of 31.5, was extruded with a single billet preheating temperature, 500 °C, and five different ram speeds, 2 mm/s, 5 mm/s, 10 mm/s, 15 mm/s, and 20 mm/s. Each profile comprised a batch of 15 billets, with the first three billets extruded to achieve steady-state process conditions. Both profiles had a ram acceleration time of 5 s. In all cases, the billet material was homogenized for 2 h at 565 °C, with the extruded profiles subject to water quenching with a quench box
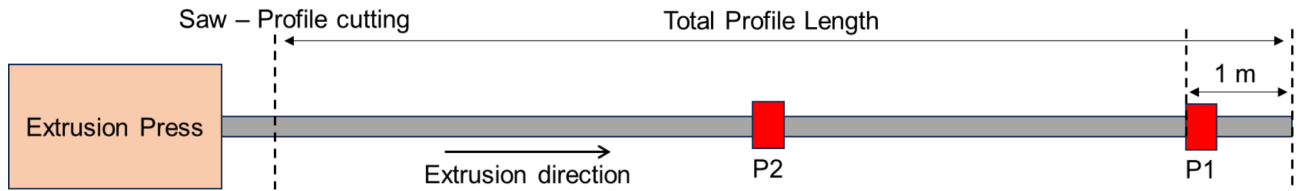
Fig. 2. Positions at which microstructural analysis was performed on both extruded profiles.
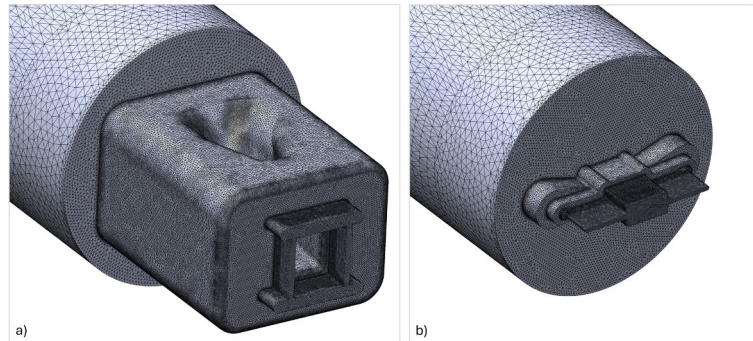
Fig. 3. FEM simulation meshes employed for (**a**) Profile A and (**b**) Profile B (images generated using Solidworks 2023[31] v. SP2.1).

positioned approximately 700 mm from the die bearings. The temperature of the profile after the quench box was measured as 20 °C to assess the cooling efficiency and prevent any potential recrystallization phenomena. For both extruded profiles, data relating to the profile exit temperature and extrusion load were collected to verify the accuracy of FEM simulations developed to simulate the extrusion process in each case (see Sect. "FEM modelling"). Microstructural analysis of both profiles was performed on sections obtained at two positions, as shown in Fig. 2. The first point, P1, was located at 1 m from the head of the profile while the second, P2, was located in the central region.

Experimental grain dimensions were obtained with standard metallographic procedures. Profiles were sectioned, ground, polished and subject to electrochemical etching (15 mL HBF_4, 750 mL H_2O) with anodization at 40 V DC for 4 min. Subsequently, samples were examined under a polarized light optical microscope to reveal differences in grain orientations. Grain sizes were measured according to ASTM E112-13 at various locations on profile sections (see Fig. 7 for more details) to ensure a comprehensive and accurate representation of the microstructure for both profiles. Measurements were taken at over 20,000 points across both profiles for training and testing of the proposed prediction models. Experimental analyses included quantification of the grain size and verification of PCG formation at each point.

FEM modelling

Simulations of each extrusion were conducted using Qform Extrusion UK v. 11.1.0[29], a FEM code based on the Arbitrary-Lagrangian-Eulerian (ALE) approach. The software allows development of customized post-processing subroutines to calculate additional parameters based on standard simulation output values. Simulations were conducted in line with the methodology described in a previous work using the parameters presented in Table 2[18].

Simulations were based on a viscoplastic material model for AA6082 aluminum alloy defined by the Hensel-Spittel flow stress law. This approach directly relates flow stress to the strain, strain rate and temperature, effectively capturing the thermomechanical response of aluminum alloys under conditions of large deformation, high strain rates and elevated temperatures. To ensure comprehensive analysis, separate simulations were conducted for each specific combination of process parameters. Simulation times were 80–100 min for Profile A and 50–60 min for Profile B on a workstation with an Intel® Xeon® X5675 CPU (3.07 GHz, dual-processor configuration) and 48 GB RAM, reflecting the difference in geometric complexity of the two profiles. Particular focus was placed on definition of the mesh, which was generated directly from the CAD geometry of the die (Fig. 3). The Qshape tool within Qform Extrusion UK was employed to automatically generate an optimized mesh with tetrahedral elements. Mesh adaption factors such as size and adaption parameters within the software were set to achieve the highest possible mesh refinement to capture intricate process details. Sticking friction conditions were applied between the billet and the die, ram and container, while a Levanov friction condition was applied between the workpiece and bearings (Table 2). Optimized boundary conditions for friction and heat exchange employed within Qform Extrusion UK have been extensively validated in the literature[18,30]. The FEM model employed explicit time integration, with the time step determined dynamically based on the velocity field. Remeshing was unnecessary, even in primary deformation zones such as tool cavities and ports, as the extrusion

Friction conditions	Value/definition
Billet - die/ram/container friction	Sticking condition
Profile - bearing friction	Levanov model (m = 0.3, n = 1.25)
Flow stress law	
Flow stress equation	$\bar{\sigma} = A \bullet e^{m_1 T} \bullet \bar{\varepsilon}^{-m_2} \bullet \dot{\bar{\varepsilon}}^{-m_3} \bullet e^{\frac{m_4}{\bar{\varepsilon}}} \bullet (1+\bar{\varepsilon})^{m_5 T} \bullet e^{m_7 \bar{\varepsilon}} \bullet \dot{\bar{\varepsilon}}^{m_8 T} \bullet T^{m_9}$
A [MPa]	270
m1 [K^{-1}]	−0.0045
m2	−0.127
m3	0.13
m4	−0.016
m5 [K^{-1}]	0.00026
m7	0
m8 [K^{-1}]	0
m9	0
Material properties	
Density [Kg/m^3]	2690
Specific heat [J/kg K]	900
Thermal conductivity [W/m K]	200
Thermal expansivity [m/K]	$2.34 \times 10 - 5$
Young's modulus [GPa]	68.9
Poisson's ratio	0.33
Mesh parameters Profile A	
Workpiece elements	1,927,131
Die set elements	1,610,855
Total	3,537,986
Mesh parameters Profile B	
Workpiece elements	1,087,219
Die set elements	1,058,202
Total	2,145,421

Table 2. Qform FEM simulation parameters, flow stress law and coefficients for AA6082 aluminum alloy[18], material properties and mesh parameters.

process was quasi-stationary. This approach not only ensured accurate representation of the extrusion process but also maintained computational efficiency.

After performing simulations, the predicted extrusion load and profile exit temperature were compared with experimental data to determine the accuracy of the simulation, with the deviation between the two being consistently below 5% for both parameters.

Output parameters from the develop FEM model and a customized post-processing subroutine were exported at the same points at which grain size and PCG formation were evaluated experimentally. Parameters included the temperature, strain, maximum strain rate, stored energy, percentage dynamic recrystallization, effective stress, profile exit velocity and velocity deviation. Temperature, strain, effective stress and profile exit velocity were calculated as standard outputs from the Qform simulation, while the remaining parameters were determined using the post-processing subroutine. The maximum strain rate was calculated as described in a previous work[30], by collecting all strain rate values observed during material deformation from the billet to the profile exit section and considering only the highest value. This method accounts for the influence of the deformation path on the analyzed parameter. Values of stored energy and percentage dynamic recrystallization were calculated as described in Sect. "Analytical prediction of grain size and PCG formation", while the velocity deviation was calculated as a standard output from the FEM simulation representing the deviation from the mean value of the exit velocity.

Analytical prediction of grain size and PCG formation

Analytical models for predicting grain size and PCG formation in extruded profiles based on FEM simulation outputs have been presented in the literature[18]. For reader convenience, the main elements of these models are summarized in Table 3. Equation 1 provides an expression for calculating the stored energy, Pd, which is the energy stored in the crystal structure promoting recrystallization. This calculation depends on the parameters listed in Table 4 including the subgrain size, δ (Eq. 2), which in turn is calculated based on the Zener-Hollomon parameter, Z (Eq. 3). Equation 4 provides an expression for calculating the percentage dynamic recrystallization taking place during billet deformation, X_{DRX}, based on the critical pinch-off strain for the occurrence of dynamic recrystallization, ϵ_c, and saturation level, ϵ_s. Finally, Eq. 5 provides an expression for calculating the cross-sectional diameter of the grain, d_t, after deformation and dynamic recrystallization. As reported in

Analytical Model [1,18,30]	Constants and variables [18]
(1) $Pd = \frac{Gb^2}{10}\left[\rho i(1 - \ln(10B\rho i^{0,5})) + \frac{2\theta}{b\delta} * \left(1 + \ln\left(\frac{\theta_c}{\theta}\right)\right)\right]$	Pd : stored energy (J/mol*K) G: material shear modulus (2.05×10^{10} Pa) B: Burgers vector (2.86×10^{-10} m) ρi: internal dislocation density δ : subgrain size (µm) Θ : subgrain misorientation angle Θc: misorientation angle limit (15°) C: material constant (3.36×10–9 m^{-1}) n: material constant (5.577) Z: Zener-Hollomon parameter Q: activation energy (182000 J/mol*K) R: universal gas constant (8.341 J/mol) T: temperature (K) $\dot{\epsilon}$: maximum strain rate of point along extrusion flow path (s^{-1}) X_{DRX}: percentage dynamic recrystallization (%) β : constant (1.823) ϵ : strain ϵ_c: critical pinch-off strain (3) ϵ_s: saturation strain (16) m : constant (1.109) d_t: cross-sectional diameter of DRX grain (µm) δ_{ss}: subgrain size under steady-state conditions (6.4 µm) k_1 : material constant (0.4) d_0: billet grain diameter (µm)
(2) $\frac{1}{\delta} = C\,(ln\,(Z))^n$	
(3) $Z = \dot{\epsilon}\,exp\left(\frac{Q}{RT}\right)$	
(4) $X_{DRX} = 1 - \exp\left[-\beta\left(\frac{\epsilon - \epsilon_c}{\epsilon_s}\right)^m\right]$	
(5) $d_t = (d_0 - 2.5\,\delta_{ss})\,(k_1)^\epsilon + 2.5\,\delta_{ss}$	

Table 3. Summary of parameters employed in analytical models for predicting grain size and PCG formation in extruded profiles.

	Grid optimization	Final parameters, PCG formation	Final parameters, grain size
Activation function for fully connected layers	Rectified linear unit (ReLU); Hyperbolic tangent (tanh); Sigmoid	ReLU	Sigmoid
Number of fully connected layers	1–2	1	2
Number of neurons per layer	1–50	Layer 1: 22	Layer 1: 20 Layer 2: 20

**Table 4**. ANN hyperparameter ranges employed for grid optimization and final ANNs.

a previous work[18], PCG occurrence was predicted when the temperature, maximum strain rate and X_{DRX} exceeded critical threshold values determined via regression as 460 °C, 125 s$^{[-1}$ and 0.70, respectively. PCG layer and d_t were calculated based on the same FEM simulation outputs as employed for the developed ANN prediction models, allowing direct comparison of the performance of data-driven and analytical models.

Artificial neural network prediction of grain size and PCG formation

ANNs for prediction of grain size and PCG formation were trained and tested by considering the extrusion exit temperature, strain, maximum strain rate, stored energy, percentage dynamic recrystallization, effective stress, velocity and velocity deviation as inputs, derived from FEM simulations and the associated sub-routines. The output parameter for PCG prediction was classification of PCG occurrence ('yes') or not ('no'), while the output parameter for grain size prediction was the grain size itself. The final dataset was randomly partitioned into 80% training and 20% test sets, with the latter employed to verify the accuracy of each trained ANN. Grain size prediction was not performed within regions of PCG formation as this was highly variable and unreliable to predict, further to being of limited interest once the PCG defect was detected.

PCG prediction was performed by training feedforward fully connected neural networks for classification with the *fitcnet* function in MATLAB. Similarly, grain size prediction was performed by training feedforward fully connected neural networks for regression with the *fitrnet* function. Both functions employ the Broyden-Fletcher-Goldfarb-Shanno quasi-Newton algorithm (LBFGS) to minimize loss, defined as cross-entropy for classification and mean squared error (MSE) for regression. Data standardization was performed in all cases. ANN layer weights were initialized with the Glorot initializer, while the initial bias of all fully connected layers was zero. To obtain detailed insight into the effects of the number of hidden layers, number of neurons per hidden layer and activation functions on the test set loss in each case, grid hyperparameter optimization was performed over the ranges shown in Table 4. Optimal ANN hyperparameters for prediction of PCG formation and grain size are listed in the same table, with schematics of the two configurations shown in Fig. 4.

Once optimal ANN configurations were identified, trained ANNs for prediction of grain size and PCG formation were utilized to produced PCG and grain size maps for each of the employed experimental conditions based on data obtained from FEM simulations and associated sub-routines, allowing qualitative comparison with the experimentally acquired microstructure and providing an example of how the methodology could be employed in a real production environment.
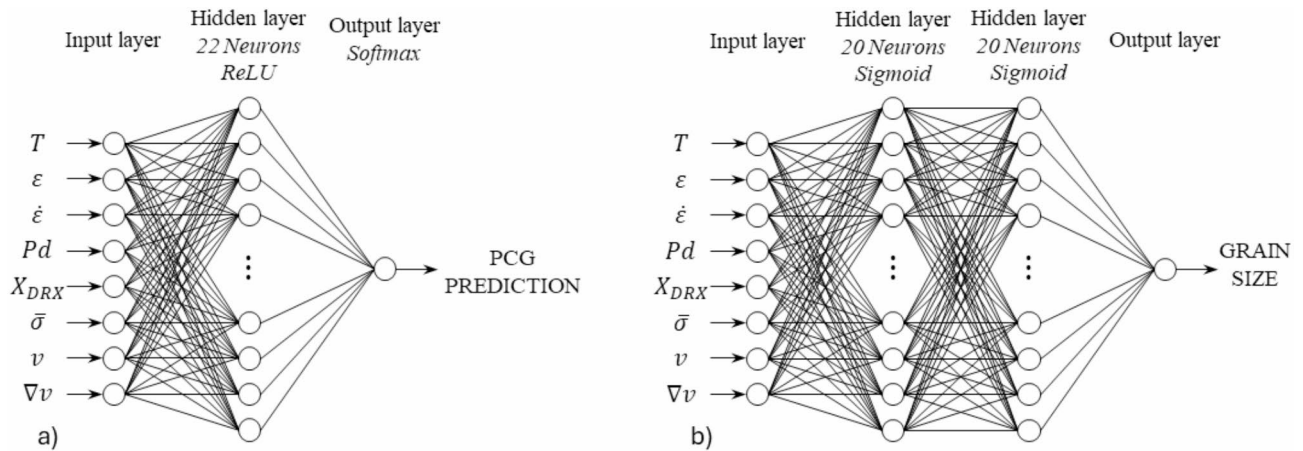
Fig. 4. Schematic of final ANN configurations employed for (**a**) PCG and (**b**) grain size prediction.

Results and discussion
Extrusion and micrograph analysis
Figure 5 displays micrographs obtained at positions P1 and P2 (Fig. 2) on Profile A obtained with a billet preheating temperature of 450 °C and ram speeds of 2 mm/s, 5 mm/s and 10 mm/s. The inset on the righthand side provides a higher magnification image of the PCG defect, appearing as a layer of recrystallized grains along the edges of the extruded profile that are significantly larger than fibrous grains at the center. The main observation that could be made from this analysis was that the extent of the PCG defect was proportional to the increase in extrusion speed, with the layer consistently expanding as the ram speed increased. Additionally, there were no significant differences in PCG extent between points P1 and P2, suggesting that a steady-state process condition was achieved at both locations. The same trend can be observed in the micrographs of the same profile obtained with a billet preheating temperature of 500 °C (Fig. 6) suggesting that the extrusion speed had a more significant influence on PCG formation than variations in billet preheating temperature, an outcome that has been analyzed and discussed in previous works[18].

Micrographs obtained at positions P1 and P2 on Profile B were virtually identical, for which only those obtained at position P2 are shown in Fig. 7. A direct correlation can again be observed between the extent of the PCG layer and ram speed up to 10 mm/s, after which the PCG thickness remains relatively constant, even as the ram speed is doubled. It can be observed that the PCG thickness at the end of each lateral fin does not follow the same trend, increasing up to a ram speed of 10 mm/s but then decreasing between 10 and 20 mm/s. It is possible that this outcome was due to imbalance in exit velocities within the profile section caused by incorrect die design, which will be discussed further in Sect. "FEM modelling".

The same micrographs were used to collect experimental data for development of ANNs for prediction of grain size and PCG formation. Figure 8 displays grids superimposed on the two profiles, where the intersections of vertical and horizontal lines were used to define the positions at which the presence of PCG and grain sizes were evaluated experimentally. The grids were designed to ensure collection of adequate and representative data across the entire surface of both profiles. Specifically, a finer grid was employed near the edges of both profiles and in the seam weld zones of Profile A.

The frequency of grain sizes within regions in which PCG formation was not observed are presented in Fig. 9. As noted previously, grain size prediction was not performed within regions of PCG formation as this was highly variable and unreliable to predict. This is because regions affected by PCG undergo grain coarsening, which is considered a static phenomenon unrelated to dynamic recrystallization taking place during extrusion. In contrast, the microstructure in areas not affected by PCG reflects the effects of material deformation and dynamic recrystallization, resulting in most values of grain size falling within the range 10–40 μm, typical of AA6082 extruded profiles[2], with only a few values extending up to 60 μm.

FEM modelling
An example of output parameters from the FEM model and associated subroutine is displayed in Fig. 10 for Profile A extruded with a billet preheating temperature of 500 °C and an extrusion speed of 10 mm/s. The temperature field shows a nearly uniform distribution in the extruded material, with higher values concentrated along the outer regions due to frictional heating and plastic deformation. The plastic strain is localized at the contact interfaces, indicating significant material flow and deformation near the tooling surfaces. The maximum strain rate follows a similar pattern, with the highest values concentrated at the edges where the material undergoes the most intense shear deformation. The stored energy distribution highlights regions of high dislocation density, primarily along the periphery of the extruded section. The X_{DRX} parameter reveals a strong correlation with strain and temperature, with dynamic recrystallization occurring preferentially at the most deformed regions. The effective stress appears relatively uniform, with slight variations due to inhomogeneous deformation. The exit velocity confirms a stable material outflow, while the velocity deviation remains low, suggesting minimal flow disturbances and ensuring uniform extrusion quality.
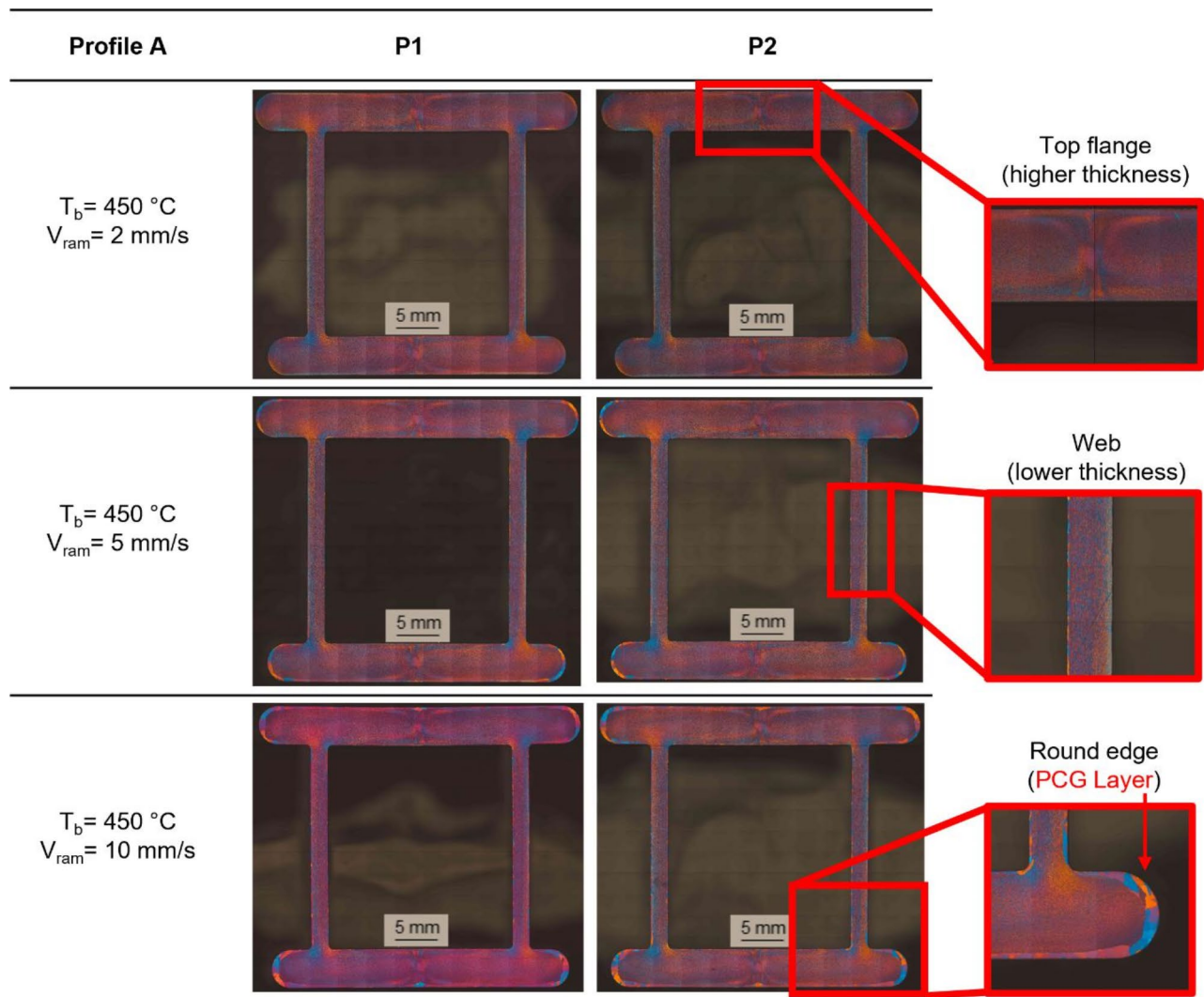
Fig. 5. Microstructural analysis of Profile A, 450 °C billet temperature.

Figure 11 provides a detailed overview of the frequency distributions of key parameters obtained from the FEM simulations, with each histogram representing the distribution of a specific parameter across the entire extrusion process. Temperature data, for example, range from 480 to 580 °C, with highest frequency between 540 and 560 °C. This temperature range is consistent with conditions typically observed in the extrusion of AA6XXX aluminum alloys. The plastic strain distribution exhibits a well-defined peak around 8, after which the frequency gradually decreases. The "More" column incorporates a range of higher strain values associated with isolated regions of particularly intense deformation. The maximum strain rate distribution is characterized by a peak at approximately 20 s^{-1} and decreasing frequency at higher values. In this case, the "More" column represents instances of extreme maximum strain rates, up to 4032 s^{-1}, occurring in isolated regions such as near seam welds or along the outer edges of the extruded profiles. The stored energy distribution is concentrated between 220 and 700 kJ/(mol·K), with a dominant peak between 340 and 400 kJ/(mol·K), reflecting the thermal energy accumulated during deformation. This stored energy is a driving force for subsequent microstructural evolution such as recovery and recrystallization. The percentage dynamic recrystallization exhibits a relatively uniform distribution with a minor peak corresponding to full recrystallization (100%) in areas experiencing highest deformation, as confirmed by strain data presented in Fig. 10 for Profile A. Effective stress values, indicative of the internal resistive forces per unit area within the material, range from 15 to 42 MPa. A significant clustering of data is evident between 15 and 21 MPa, suggesting that a substantial portion of the material experiences stresses within this interval during extrusion. The exit speed is characterized by three distinct peaks at 50, 100 and 200 mm/s, corresponding to ram speeds of 2, 5 and 10 mm/s, respectively. Velocity deviation analysis indicates that Profile A maintains a deviation close to 0%, signifying well-balanced material flow and uniform exit velocities across the entire profile cross-section. Such uniformity is indicative of an optimized die design. In contrast, Profile B demonstrates a wider distribution of velocity deviations, particularly at the extremities of the fins as illustrated in Fig. 12. Such deviations suggest localized variations in material flow, potentially resulting from die design complexity or uneven friction conditions. These irregularities can lead to defects such as PCG.
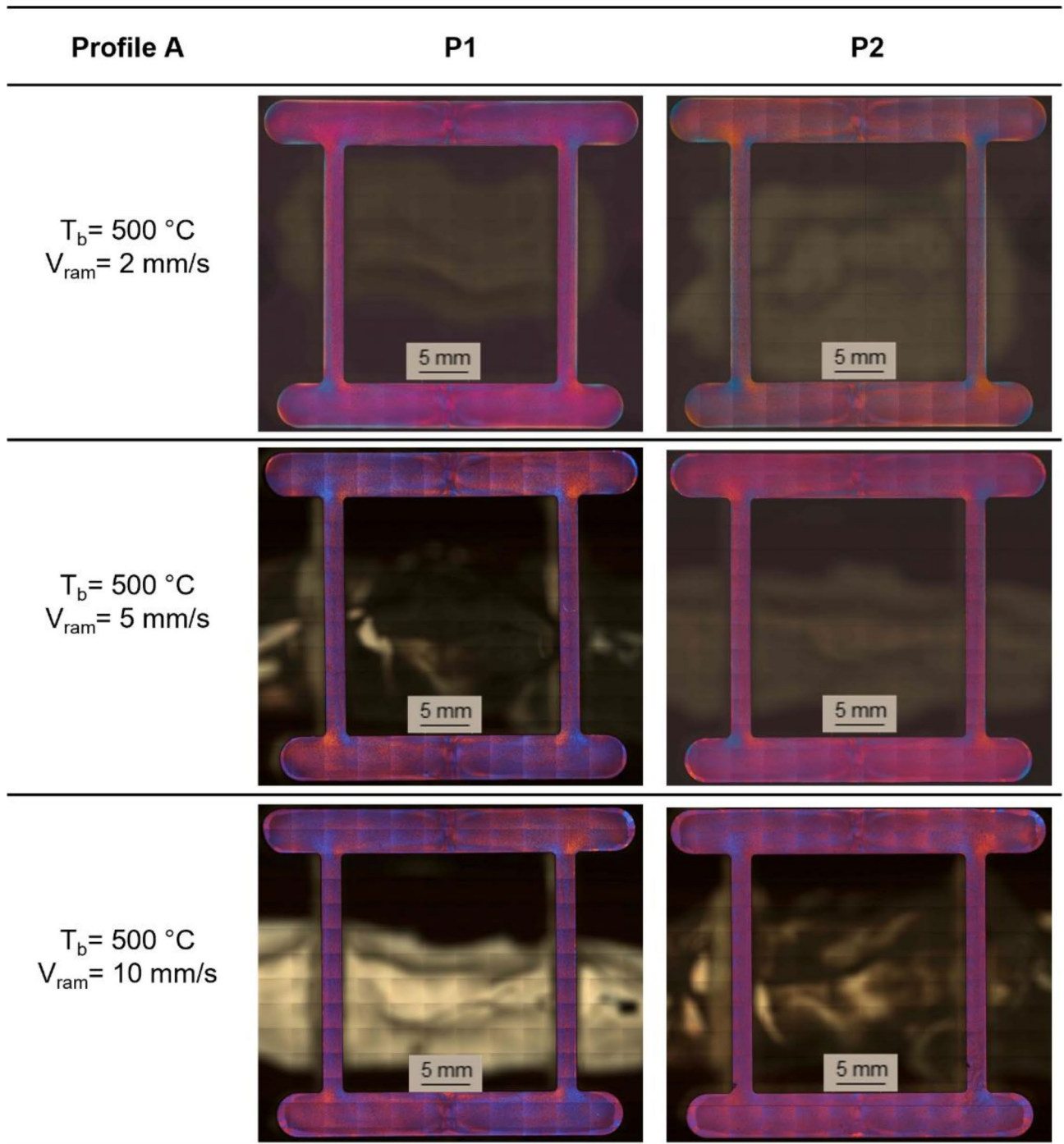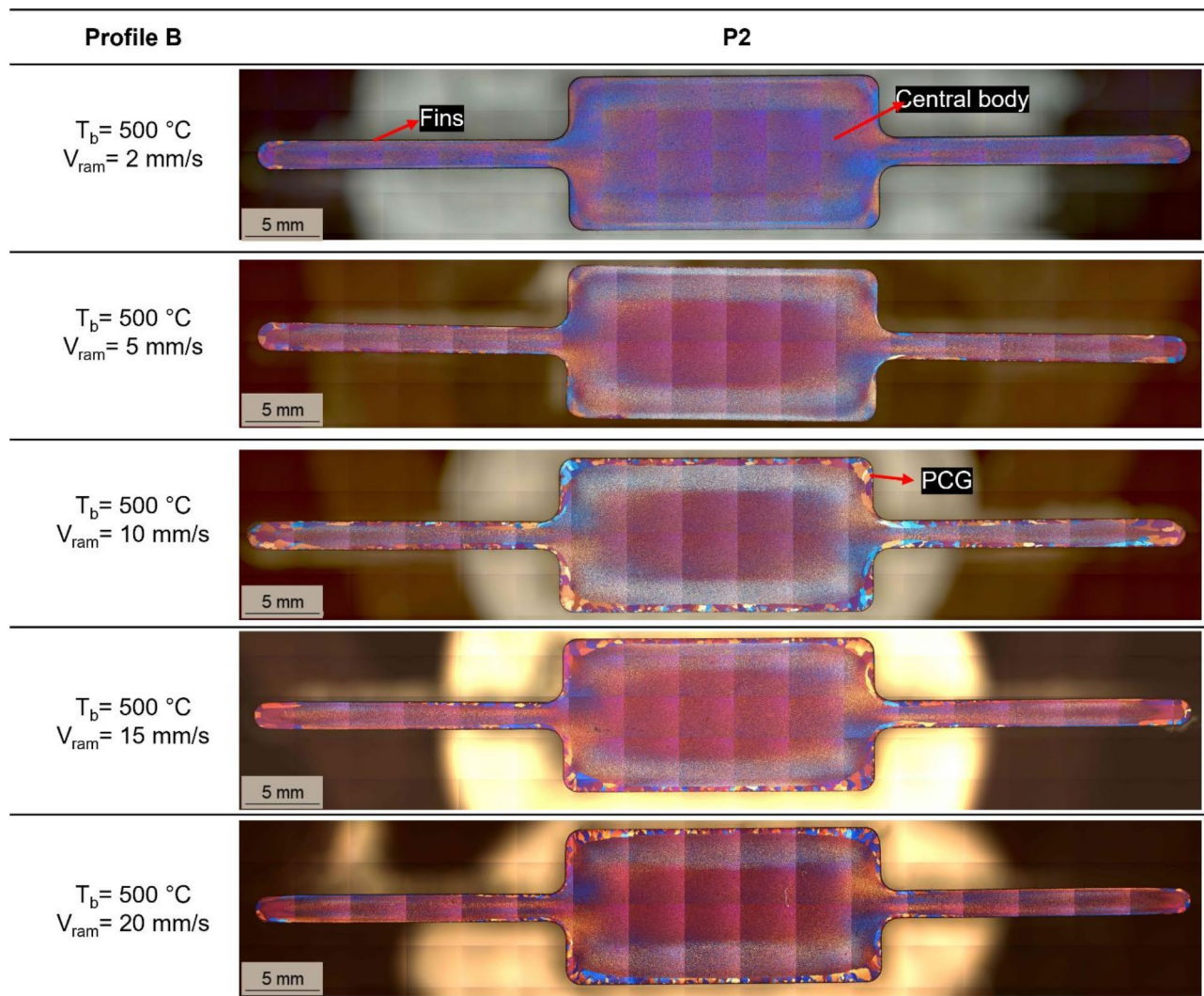
Fig. 6. Microstructural analysis of Profile A, 500 °C billet temperature.

This phenomenon is confirmed by observations presented in Fig. 7, where anomalous PCG is evident at the ends of fins.

Prediction of grain size and PCG formation

The outcomes of ANN hyperparameter optimization for prediction of PCG formation are presented in Fig. 13, where the cross-entropy (loss) of predictions in the test set is displayed as a function of the number of neurons per hidden layer for both one- and two-layer ANNs with ReLU, Sigmoid and tanh activation functions. For a single hidden layer, the loss was found to decrease with increasing neurons for all activation functions down to approximately 0.05 with 20 neurons, after which minor oscillations were observed but no further reductions were achieved. With two hidden layers, loss was strongly dependent on the number of neurons in the first layer for all activation functions down to approximately 0.05 for 20 neurons, while the outcome was virtually independent of the number of neurons in the second layer except for very high values, where loss increased with ReLU and tanh

Fig. 7. Microstructural analysis of Profile B, 500 °C billet temperature.

activation functions. With no improvement in ANN accuracy observed with two hidden layers, a single hidden layer was selected for the final model. Although all activation functions performed similarly, an ANN with 22 neurons and a ReLU activation function was selected for the final configuration due to the threshold type nature of PCG formation and the slightly lower variability of observed outcomes during hyperparameter optimization.

The outcomes of PCG prediction in the test set with the final trained ANN (Table 4) and analytical model (Table 3) are presented in Fig. 14. Significantly lower error rates were observed with the ANN than with the analytical model. The former yielded 5.8% false negatives compared to 10.1% with the analytical model and 3.9% false positives compared to 18.1%. Prediction of PCG formation with the ANN model was therefore found to be far more reliable than the analytical model.

The outcomes of ANN hyperparameter optimization for prediction of grain size are presented in Fig. 15, where the MSE of predictions in the test set is displayed as a function of the same hyperparameters. Outcomes were somewhat different to those observed for PCG prediction, with clear distinction between the performance of ANNs with one and two hidden layers. In the former case, the MSE decreased steadily with increasing number of neurons for all activation functions down to approximately 11–12 μm^2 with 50 neurons. With two hidden layers, further reductions in MSE were observed down to approximately 9 μm^2 with at least 20 neurons in both hidden layers and a Sigmoid activation function. Loss was strongly dependent on the number of neurons in the first layer for all activation functions and moderately dependent on the number of neurons in the second layer. Variability of results was somewhat high where the latter was less than 10. Differences could also be observed between the various activation functions, with Sigmoid yielding lowest MSE and variability and tanh presenting the highest of both. An ANN with two hidden layers containing 20 neurons each and a Sigmoid activation function was selected for the final ANN configuration, as this was found to be the simplest configuration that could reliably achieve an MSE of less than 10 μm^2.

The outcomes of grain size prediction in the test set with the final trained ANN (Table 4) and analytical model (Table 3) are presented in Fig. 16 for regions in which PCG formation was not observed. The trained ANN
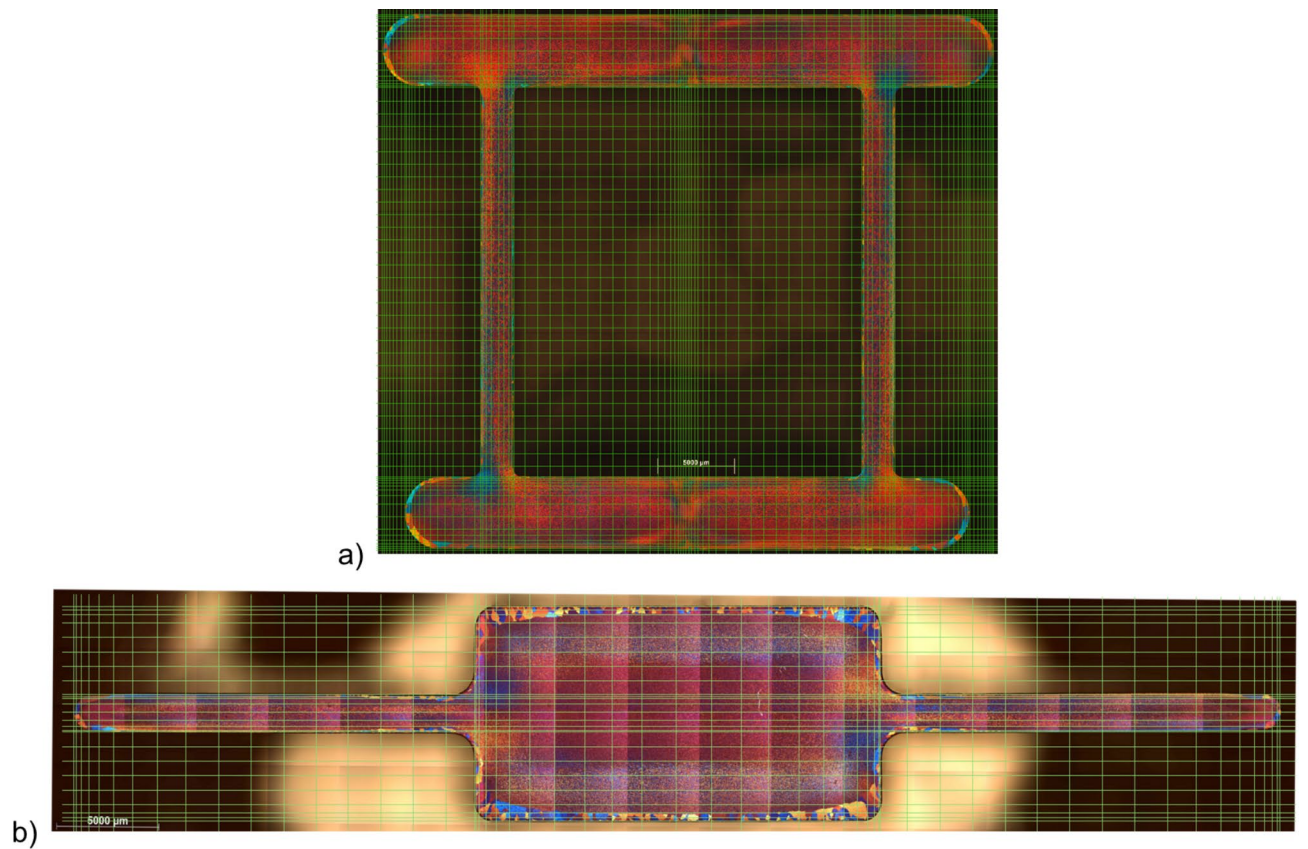
Fig. 8. Grids used to define the positions at which the presence of PCG and grain sizes were evaluated experimentally (**a**) Profile A and (**b**) Profile B.
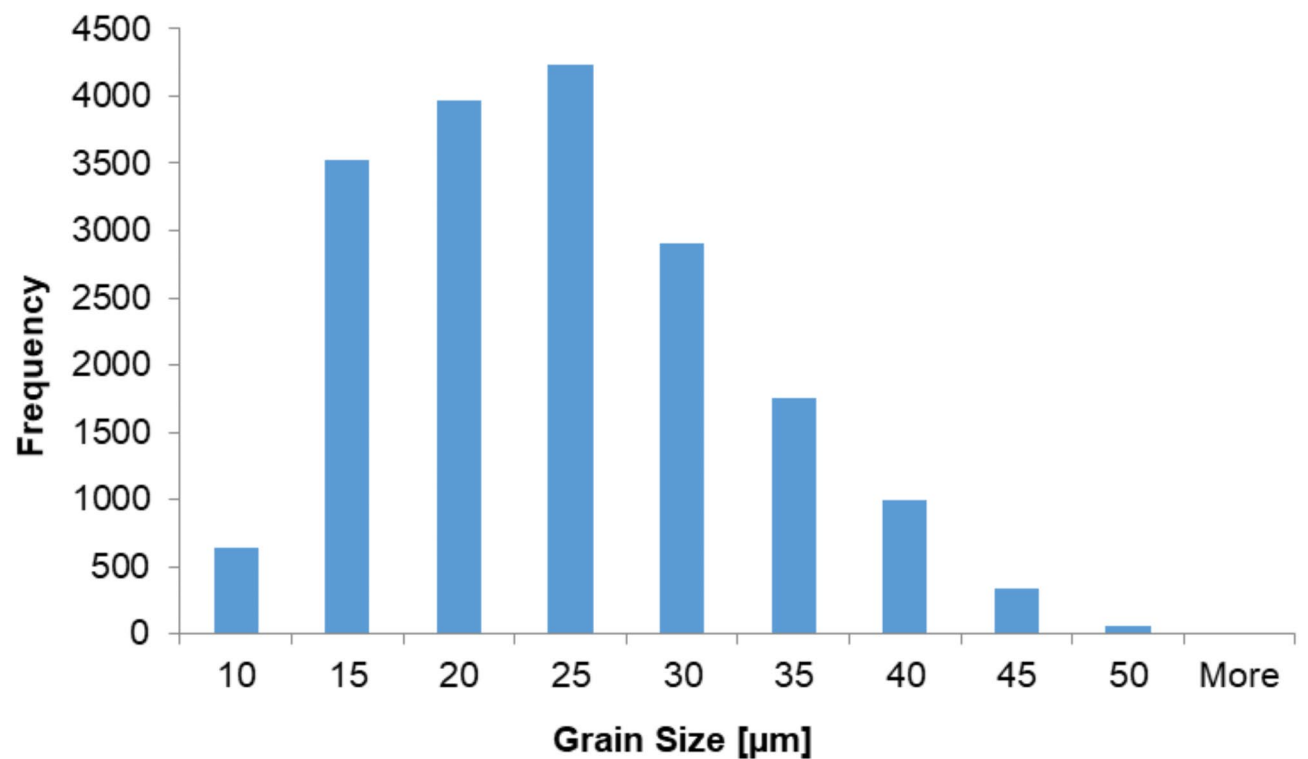

Fig. 9. Frequency of the experimental grain size data.
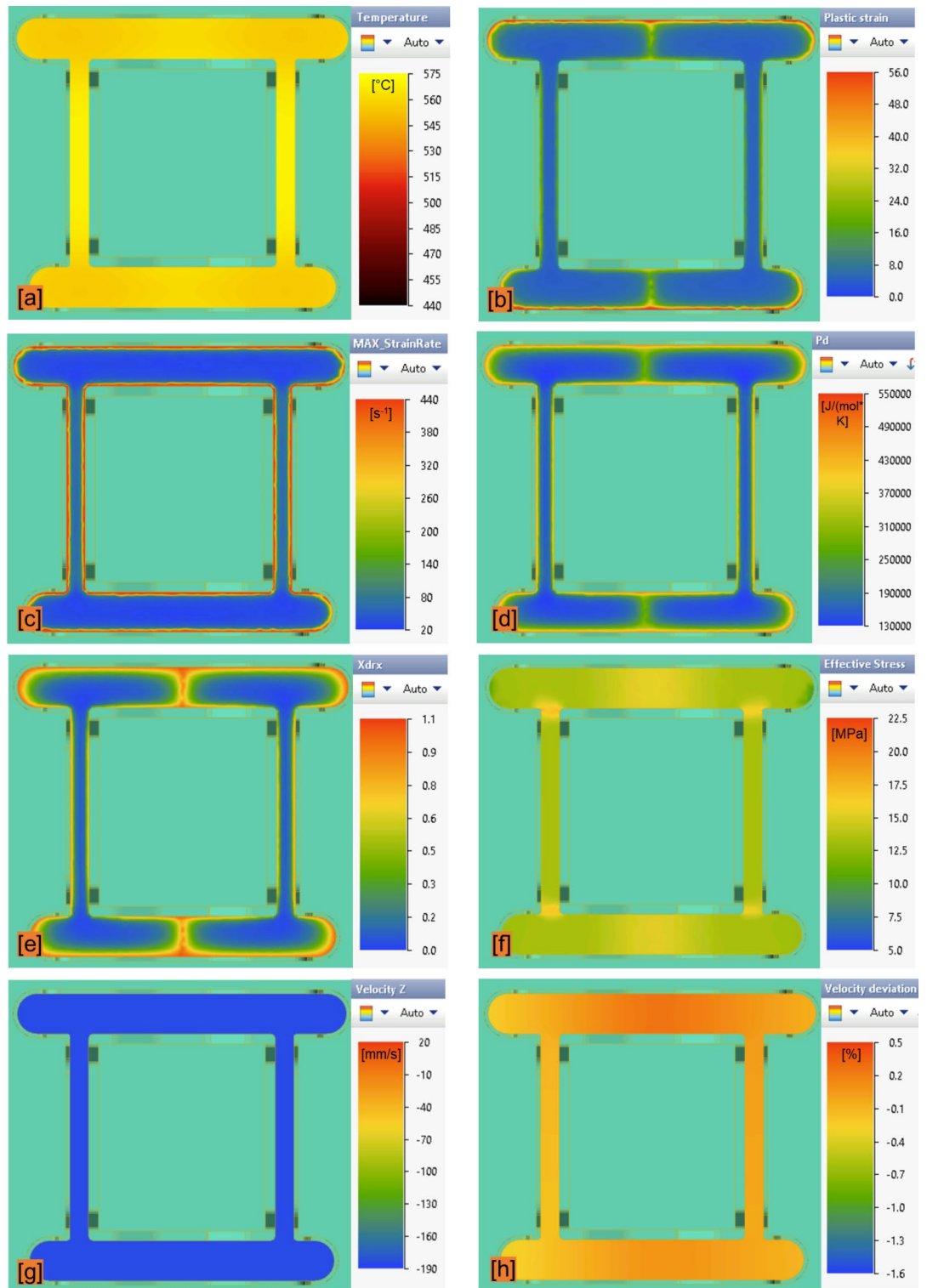
Fig. 10. FEM simulation results for Profile A extruded with a billet preheating temperature of 500 °C and an extrusion speed of 10 mm/s: (**a**) temperature, (**b**) plastic strain, (**c**) maximum strain rate, (**d**) stored energy, (**e**) X_{DRX}, (**f**) effective stress, (**g**) exit velocity, (**h**) velocity deviation.

predicted the grain size with an MSE of 9.77 μm^2, mean absolute percentage error (MAPE) of 10.9% and a total of 91.1% points with an absolute percentage error less than 25%. In contrast, the analytical model achieved an MSE of 48.3 μm^2, MAPE of 22.7% and 59.1% of points with an absolute percentage error of less than 25%. The ANN therefore provided far higher accuracy than the analytical model for predicting grain size in the present case. As discussed in Sect. "Analytical prediction of grain size and PCG formation", the analytical model was based
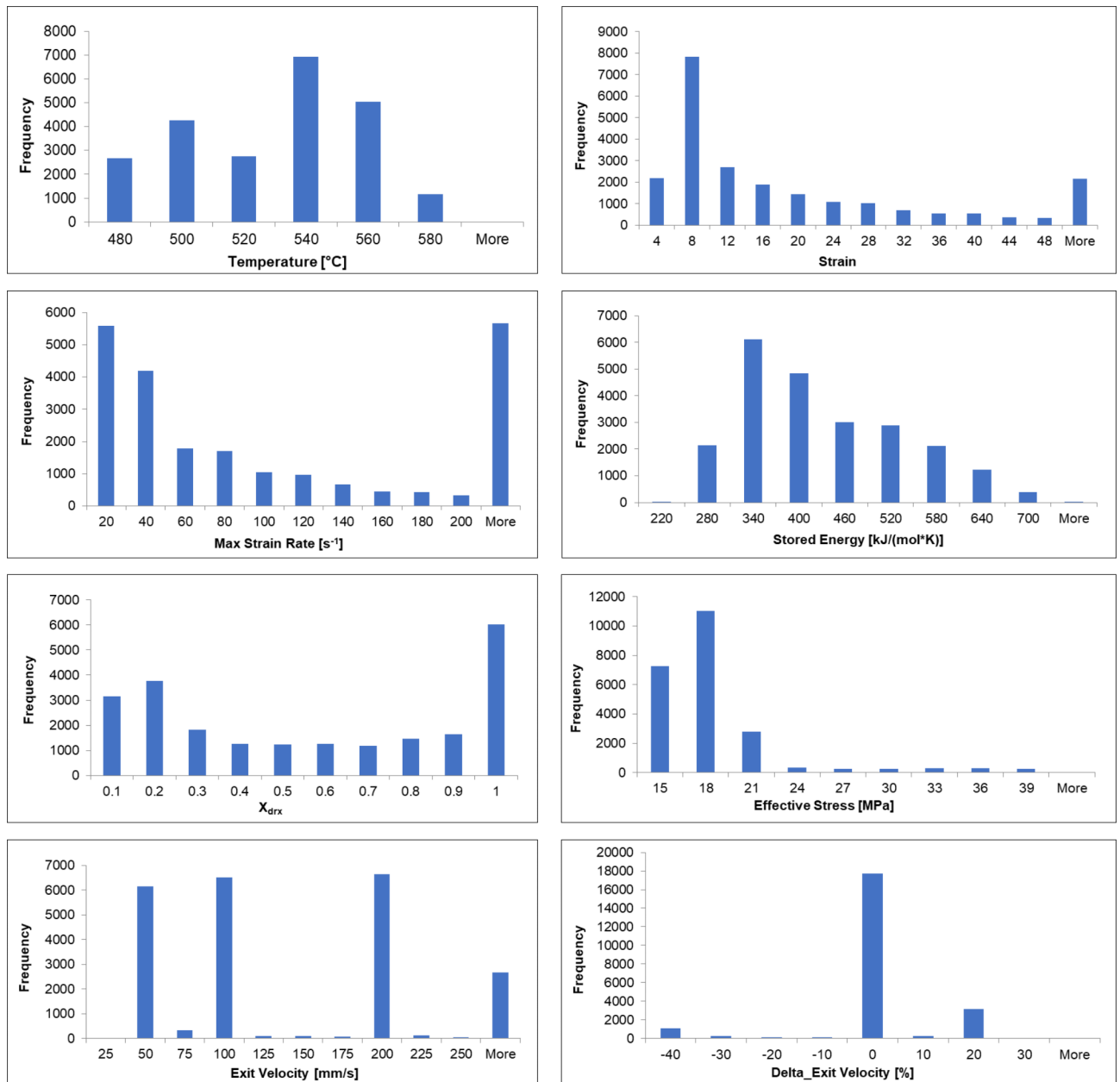
Fig. 11. Frequency of the FEM simulation outcomes for entire dataset (both investigated profiles).

on Eq. 5, calculating the diameter of the recrystallized grain as the sum of two terms: $(d_0 - 2.5\,\delta_{ss})\,(k_1)^\epsilon$ and $(2.5\,\delta_{ss})$. The first term approaches zero at high strain values, while the second is a constant that identifies the minimum grain diameter. By observing the results of the analytical model in the present case, it is clear that there was a decrease in accuracy due to regions characterized by high strain values, resulting in a relatively large number of points where the first term in Eq. (5) was negligible but the experimental grain size was relatively large. Although it is likely that the analytical model could be improved by better accounting for regions of high strain, this falls beyond the scope of the present work.

PCG and grain size mapping

Predicted PCG and grain size maps are presented, together with experimental micrographs of all tested profiles, in Figs. 17, 18 and 19 for Profile A with billet preheating temperatures of 450 °C and 500 °C and Profile B with a billet temperature of 500 °C. Regions in which PCG formation was predicted are displayed in black within the righthand images, with the color representing the grain size within the remaining area. Although it is qualitatively challenging to compare the numerical grain sizes with the experimentally reported micrographs due to the small sizes involved (a quantitative comparison is nonetheless provided in Fig. 16), a qualitative comparison can instead be made regarding the prediction of PCG.
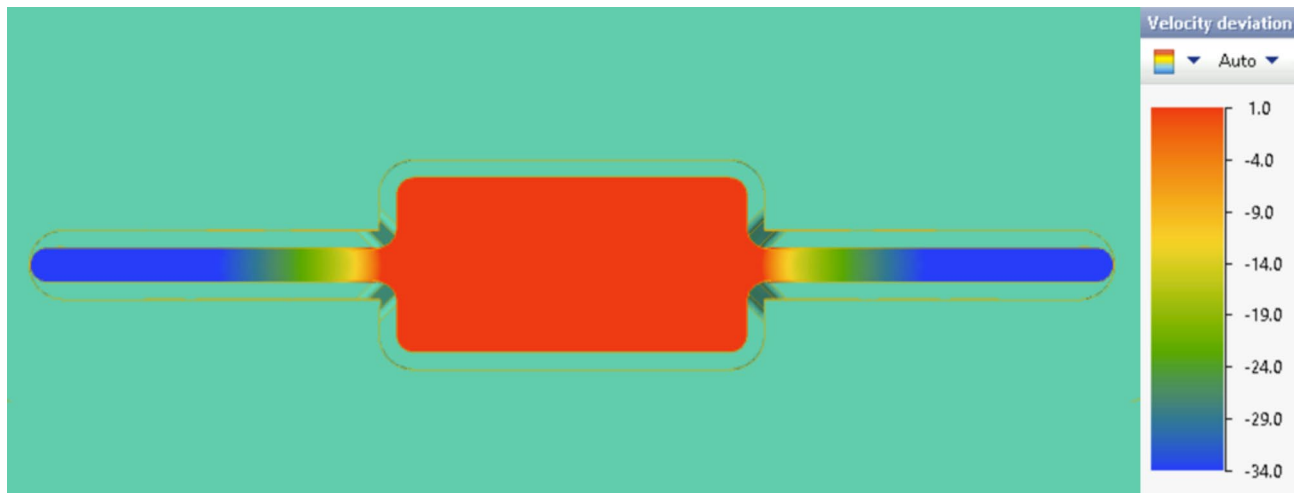
**Fig. 12**. Simulated velocity deviation for Profile B.
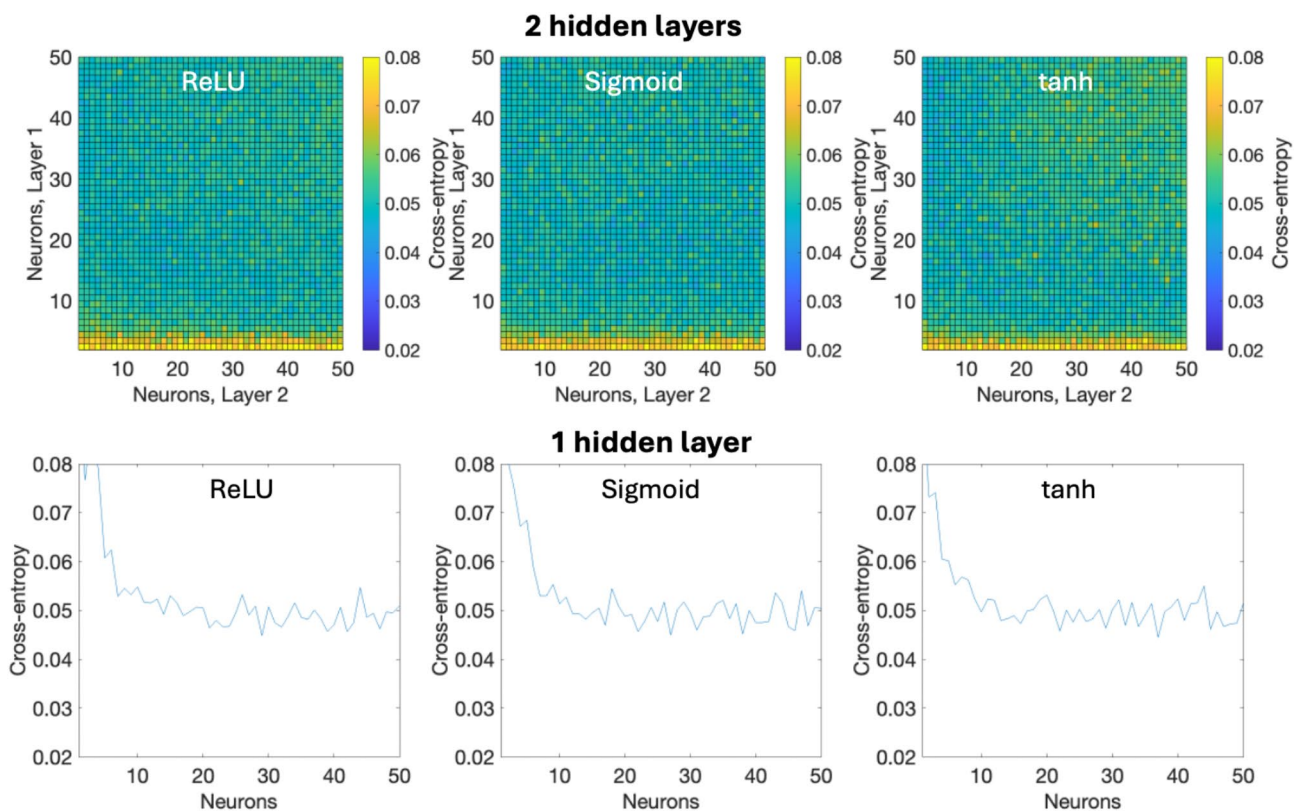
Fig. 13. ANN hyperparameter optimization for PCG prediction: cross-entropy loss in test set as a function of the number of neurons per layer for one and two-layer configurations with ReLU, Sigmoid and tanh activation functions.
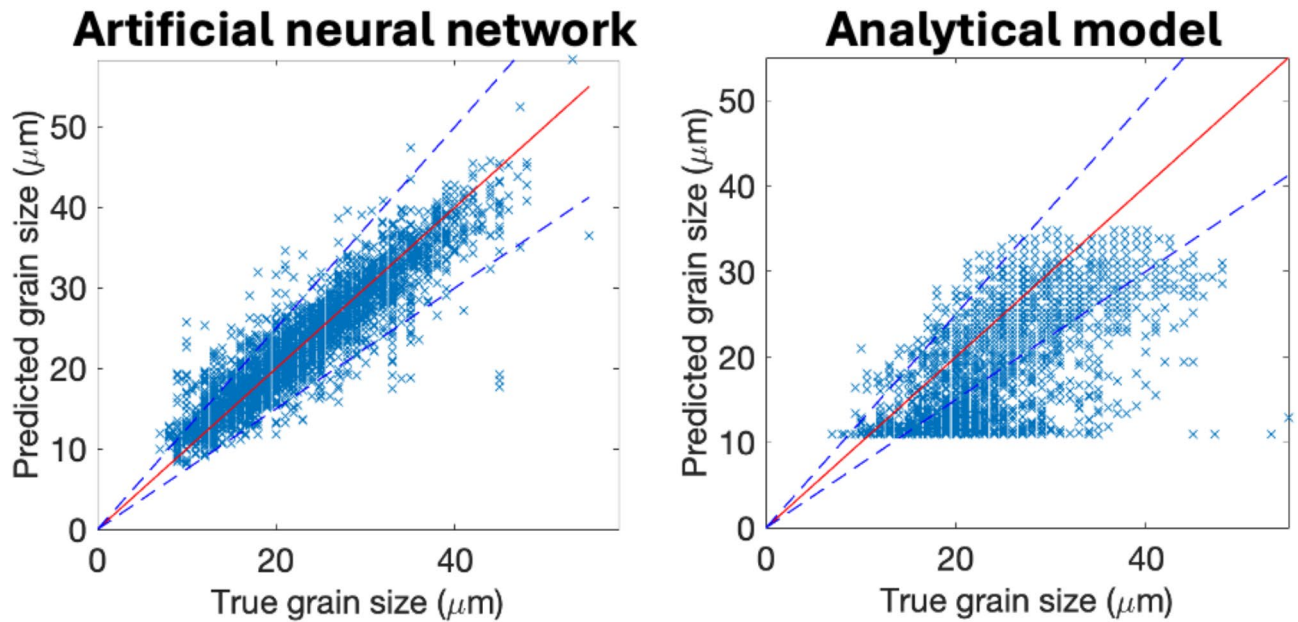
Comparison of the predicted and experimental results for Profile A extruded with a billet preheating temperature of 450 °C (Fig. 17) shows excellent correspondence between the experimentally recrystallized layer and that predicted by the ANN, both in terms of PCG layer growth with ram speed and the positions in which it forms within the profile. Specifically, it can be observed that formation of PCG takes place more prominently at the edges of the horizontal sides and at the outer edge, while less so and intermittently at the inner edges, consistent with experimental outcomes. The same trend can be observed for Profile A extruded with a billet preheating temperature of 500 °C (Fig. 18), with PCG absent in the profile at 2 mm/s, while at 5 mm/s a thin layer
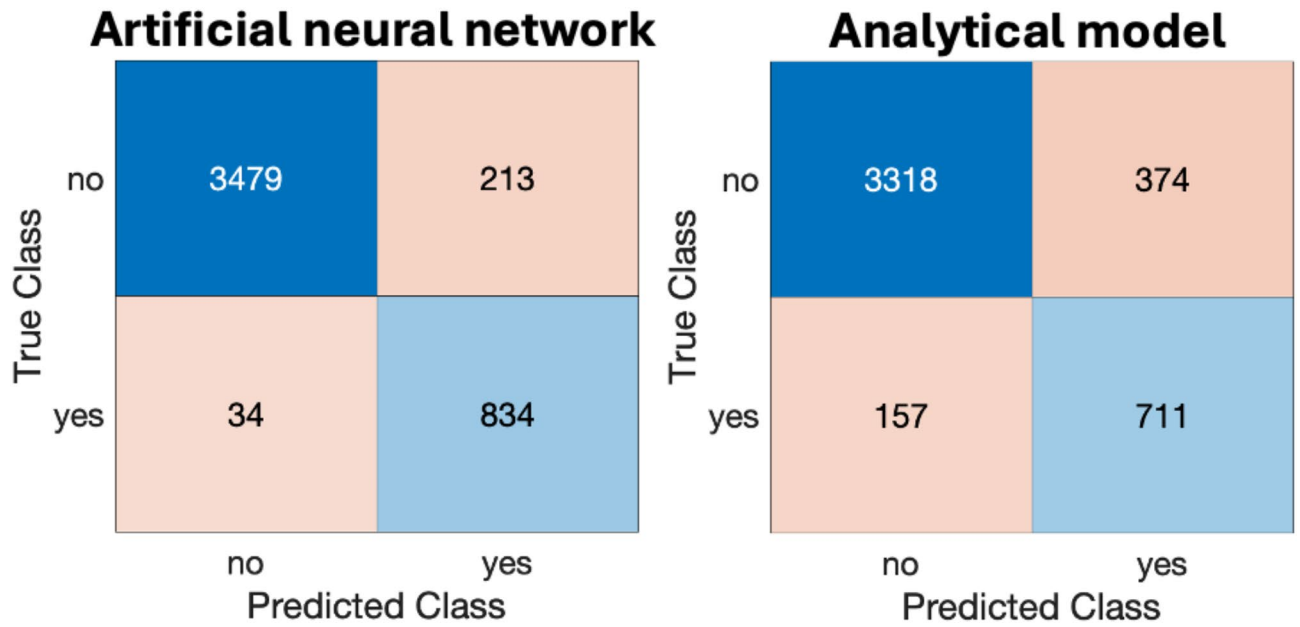
Fig. 14. Confusion matrices of PCG prediction in test dataset with final trained ANN (Table 4) and analytical model (Table 3). yes = PCG formation; no = no PCG formation.
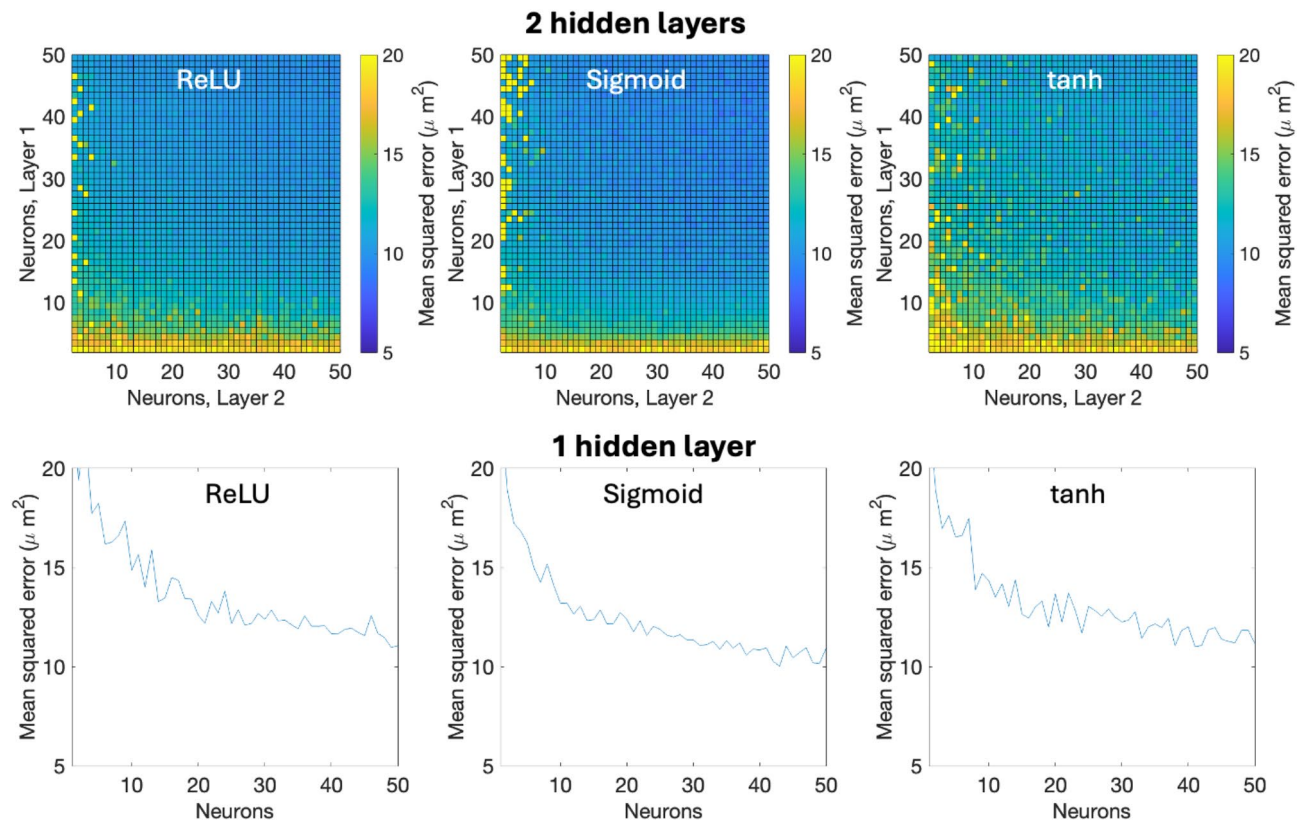
Fig. 15. ANN hyperparameter optimization for grain size prediction: MSE in test set as a function of the number of neurons per layer for one and two-layer configurations with ReLU, Sigmoid and tanh activation functions.

Fig. 16. Predicted vs. true grain size in test dataset with final trained ANN (Table 4) and analytical model (Table 3), together with mean predictor importance of trained ANN. Dashed blue lines represent 25% absolute percentage error.
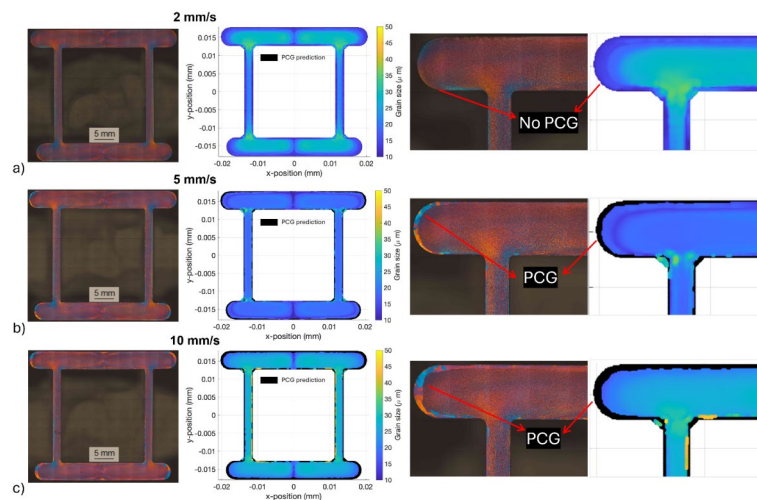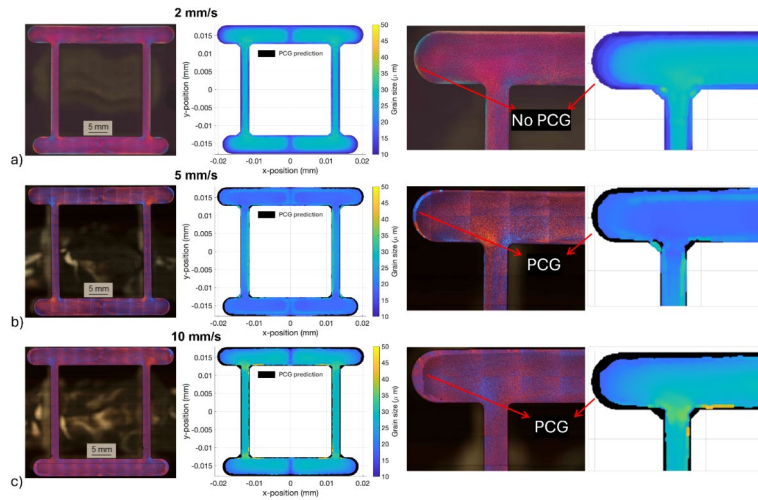

Fig. 17. Comparison of predicted PCG and grain size maps with micrographs for profile A extruded with a billet preheating temperature of 450 °C: (**a**) 2 mm/s, (**b**) 5 mm/s, (**c**) 10 mm/s. PCG formation shown in black.

appears at the edges of the horizontal sides. This layer then grows consistent with experimental observations as the ram speed increases to 10 mm/s.

Comparison of the predicted and experimental results for Profile B (Fig. 19) again shows good correspondence between the experimental PCG extent and that predicted by the ANN. At a ram speed of 2 mm/s, the ANN predicts no PCG defect, while at 5 mm/s, a small and intermittent defect begins to appear, which becomes thicker as the speed increases to 10 mm/s. The thickness remains almost constant in the central solid rectangular section as the ram speed increases, except at 20 mm/s, where the ANN accurately predicts a slight reduction in the PCG layer within this region as well as a decreasing trend within the fins. This outcome illustrates that the ANN can accurately predict the PCG defect not only within the central area but also within the fins, where an unbalanced velocity distribution was observed, as discussed in Sect. 3.2.

These results have important implications for both die design and process optimization, where FEM simulations are commonly employed to predict outcomes and reduce the number of experiments to be performed to save time and cost. Employing data-driven models for predicting grain size and PCG formation represents an additional post-processing step that can be implemented relatively easily and at little cost while

Fig. 18. Comparison of predicted PCG and grain size maps with micrographs for profile A extruded with a billet preheating temperature of 500 °C: (**a**) 2 mm/s, (**b**) 5 mm/s, (**c**) 10 mm/s. PCG formation shown in black.
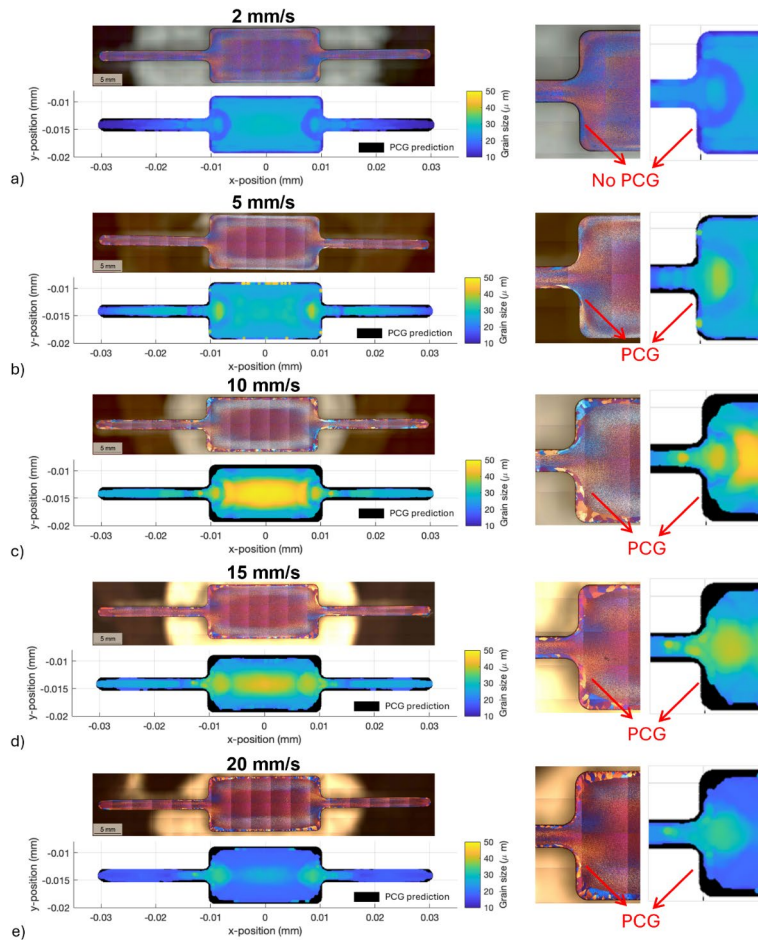
Fig. 19. Comparison of predicted PCG and grain size maps with micrographs for profile B extruded with a billet preheating temperature of 500 °C: (**a**) 2 mm/s, (**b**) 5 mm/s, (**c**) 10 mm/s, (**d**) 15 mm/s, (**e**) 20 mm/s. PCG formation shown in black.

adding significant value to the process chain. Accurate prediction of PCG formation, in particular, would allow conditions leading to this effect to be avoided during testing for process parameter optimization, while assisting in the identification of optimal conditions in terms of microstructure and throughput.

Conclusion

Prediction of Peripheral Coarse Grain (PCG) defects and grain size in extruded aluminum alloy profiles for the automotive industry represents a valuable tool for improving production efficiency by reducing the time and cost associated with die design and allowing more thorough process optimization to achieve acceptable outcomes while maximizing production efficiency. By combining FEM simulations with artificial neural networks (ANN) and experimental data from over 22,000 data points on two AA6082 aluminum alloy profiles with different geometries, extruded with various billet pre-heating temperatures and ram speeds, it was possible to demonstrate a significant improvement in prediction accuracy compared to current state-of-the-art analytical models. PCG formation was predicted with a fully connected ANN for classification, achieving 5.8% false negatives and 3.9% false positives in the test data set compared to 10.1% and 18.1%, respectively, with the analytical model, while grain size was predicted with a fully connected ANN for regression, achieving a mean squared error (MSE) of 9.77 μm^2 compared to 48.3 μm^2 with the analytical model. PCG and grain size maps were produced with trained ANNs using input data from FEM simulations and associated sub-routines, providing a demonstration of how grain size and PCG formation could be predicted in a real production environment. The models consistently predicted the growth and distribution of the PCG layer and grain size with good accuracy, aligning closely with micrographs of the same sections.

Experimental analysis of the extruded profiles revealed that the PCG layer generally increased in thickness with increasing ram speed, with the trend being consistent across different positions within the tested profiles at both 450 °C and 500 °C billet preheating temperatures. However, a unique phenomenon was observed in one of the profiles (Profile B), where the thickness of the PCG layer increased with ram speed up to 10 mm/s and then decreased between 10 and 20 mm/s, potentially due to an imbalance in exit speeds caused by the die design. The ANN model for PCG prediction was able to capture this complexity, effectively accounting for the nuanced effects of unbalanced velocity distributions on PCG formation, a challenge that conventional methods struggled to address. The accuracy of the ANN model for grain size prediction instead underscores its potential for fine-tuning extrusion parameters to achieve a desired microstructure. These outcomes suggest that combined FEM and data-driven prediction models have much potential, with effort now required to develop guidelines for the definition of efficient training datasets to maximize their effectiveness.

Data availability
Data is provided within the manuscript or supplementary information files.

References
1. Donati, L., Segatori, A., El Mehtedi, M. & Tomesani, L. Grain evolution analysis and experimental validation in the extrusion of 6XXX alloys by use of a lagrangian FE code. *Int. J. Plast.* **46**, 70–81 (2013).
2. Parson, N., Fourmann, J. & Beland, J. F. Aluminum extrusions for automotive crash applications. in 2017-01-1272 (2017). https://doi.org/10.4271/2017-01-1272
3. Rios, P. R., Siciliano Jr, F., Sandim, H. R. Z., Plaut, R. L. & Padilha, A. F. Nucleation and growth during recrystallization. *Mater. Res.* **8**, 225–238 (2005).
4. Rakhmonov, J., Liu, K., Rometsch, P., Parson, N. & Chen, X. G. Effects of Al(MnFe)Si dispersoids with different sizes and number densities on microstructure and ambient/elevated-temperature mechanical properties of extruded Al–Mg–Si AA6082 alloys with varying Mn content. *J. Alloys Compd.* **861**, 157937 (2021).
5. Goik, P., Schiffl, A. & Höppel, H. W. Formation of peripheral coarse grain in Thin-Walled Al–Mg–Si extrusion profiles. *Metall. Mater. Trans. A* **54**, 3940–3956 (2023).
6. Liu, F. et al. Effect of Mn/Cr ratio on precipitation behaviors of α-Al(FeMnCr)Si dispersoids and mechanical properties of Al–Mg–Si–Cu alloys. *Mater. Sci. Eng. A* **860**, 144269 (2022).
7. Žist, S. et al. The Effect of Scandium on the Microstructure of the Aluminium Alloy AA 6086. *Crystals* **12**, 973 (2022).
8. Österreicher, J. A., Kumar, M., Schiffl, A., Schwarz, S. & Bourret, G. R. Secondary precipitation during homogenization of Al-Mg-Si alloys: Influence on high temperature flow stress. *Mater. Sci. Eng. A* **687**, 175–180 (2017).
9. Qian, X., Parson, N. & Chen, X. G. Effects of Mn addition and related Mn-containing dispersoids on the hot deformation behavior of 6082 aluminum alloys. *Mater. Sci. Eng. A* **764**, 138253 (2019).
10. Li, Z. et al. Improved distribution and uniformity of α-Al(Mn,Cr)Si dispersoids in Al-Mg-Si-Cu-Mn (6xxx) alloys by Two-Step homogenization. *Metall. Mater. Trans. A* **52**, 3204–3220 (2021).
11. Eivani, A. R. & Zhou, J. Application of physical and numerical simulations for interpretation of peripheral coarse grain structure during hot extrusion of AA7020 aluminum alloy. *J. Alloys Compd.* **725**, 41–53 (2017).
12. Zhao, H. et al. Abnormal grain growth behavior and mechanism of 6005A aluminum alloy extrusion profile. *J. Mater. Sci. Technol.* **157**, 42–59 (2023).
13. Mahmoodkhani, Y., Chen, J., Wells, M. A., Poole, W. J. & Parson, N. C. The effect of die bearing geometry on surface recrystallization during extrusion of an Al-Mg-Si-Mn alloy. *Metall. Mater. Trans. A.* **50**, 5324–5335 (2019).
14. Pari, L. D. & Misiolek, W. Z. Theoretical predictions and experimental verification of surface grain structure evolution for AA6061 during hot rolling. *Acta Mater.* **56**, 6174–6185 (2008).
15. Misiolek, W. Z. & Van Geertruyden, W. R. Combined numerical simulation and microstructure characterization for prediction of physical properties in extruded aluminum alloys. *Key Eng. Mater.* **424**, 1–8 (2009).
16. Eivani, A. R., Zhou, J. & Duszczyk, J. Mechanism of the formation of peripheral coarse grain structure in hot extrusion of Al-4.5Zn-1Mg. *Philos. Mag.* **96**, 1188–1196 (2016).
17. Eivani, A. R., Jafarian, H. R. & Zhou, J. Simulation of peripheral coarse grain structure during hot extrusion of AA7020 aluminum alloy. *J. Manuf. Process.* **57**, 881–892 (2020).

18. Negozio, M., Segatori, A., Pelaccia, R., Reggiani, B. & Donati, L. Experimental investigation and numerical prediction of the peripheral coarse grain (PCG) evolution during the extrusion of different AA6082 aluminum alloy profiles. *Mater. Charact.* **209**, 113723 (2024).
19. Wuest, T., Weimer, D., Irgens, C. & Thoben, K. D. Machine learning in manufacturing: Advantages, challenges, and applications. *Prod. Manuf. Res.* **4**, 23–45 (2016).
20. Cui, C. et al. The coupling machine learning for microstructural evolution and rolling force during hot strip rolling of steels. *J. Mater. Process. Technol.* **309**, 117736 (2022).
21. Ding, C. Y. et al. An interpretable framework for high-precision flatness prediction in strip cold rolling. *J. Mater. Process. Technol.* **329**, 118452 (2024).
22. Hsiang, S. H., Kuo, J. L. & Yang, F. Y. Using artificial neural networks to investigate the influence of temperature on hot extrusion of AZ61 magnesium alloy. *J. Intell. Manuf.* **17**, 191–201 (2006).
23. Zhou, J., Li, L. X., Mo, J., Zhou, J. & Duczczyk, J. Prediction of the extrusion load and exit temperature using artificial neural networks based on FEM simulation. *Key Eng. Mater.* **424**, 241–248 (2009).
24. Bingöl, S., Ayer, Ö. & Altinbalik, T. Extrusion load prediction of gear-like profile for different die geometries using ANN and FEM with experimental verification. *Int. J. Adv. Manuf. Technol.* **76**, 983–992 (2015).
25. Abdul Jawwad, A. K. & Barghash, M. A. Evaluating the effects of process parameters on maximum extrusion pressure using a new artificial neural network-based (ANN-based) partial-modeling technique. *Int. J. Adv. Manuf. Technol.* **68**, 2547–2564 (2013).
26. Almutahhar, M. Prediction of tool failure in metal hot extrusion process using artificial neural networks. in 8–15 (2023). https://doi.org/10.21741/9781644902790-2
27. Jeong, S. H., Lee, S. H. & Won, H. I. Development of microcatheter tube extrusion angle Estimation system using convolutional neural network segmentation. *Sci. Rep.* **13**, 18468 (2023).
28. Nasrin, T., Pourali, M., Pourkamali-Anaraki, F. & Peterson, A. M. Active learning for prediction of tensile properties for material extrusion additive manufacturing. *Sci. Rep.* **13**, 11460 (2023).
29. https://www.qform3d.com
30. Negozio, M., Pelaccia, R., Donati, L. & Reggiani, B. Simulation of the microstructure evolution during the extrusion of two industrial-scale AA6063 profiles. *J. Manuf. Process.* **99**, 501–512 (2023).
31. https://www.solidworks.com
32. Sellars, C. M. & Zhu, Q. Microstructural modelling of aluminium alloys during thermomechanical processing. *Mater. Sci. Eng. A* **280**, 1–7 (2000).

Acknowledgements

Author contributions

M. N., L. D. and A. L. contributed equally to the scientific discussions, writing and revision of the manuscript. M. N. and L. D. performed microstructural analyses on extruded profiles, FEM simulations and analytical prediction of grain size and PCG formation. A. L. developed, optimized and tested ANNs for prediction of grain size and PCG.

Declarations

Competing interests

The authors declare no competing interests.

Additional information

Supplementary Information The online version contains supplementary material available at https://doi.org/10.1038/s41598-025-94884-4.

Correspondence and requests for materials should be addressed to M.N.

Reprints and permissions information is available at www.nature.com/reprints.

Publisher's note Springer Nature remains neutral with regard to jurisdictional claims in published maps and institutional affiliations.